# XANES Mo *L*-Edges and XPS Study of Mo Loaded in HY Zeolite

**E. J. Lede,[†,||] F. G. Requejo,*[,†,§] B. Pawelec,[‡] and J. L. G. Fierro[‡]**

*Departamento de Física, Facultad de Ciencias Exactas, UNLP, CC/67 1900 La Plata and IFLP(CONICET), Argentina, and Instituto de Catálisis y Petroleoquímica, CSIC, Cantoblanco, 28049 Madrid, Spain*

*Received: December 31, 2001; In Final Form: May 29, 2002*

Molybdena-containing ultrastable (HY) zeolites, prepared using several Mo precursors and activation procedures, were characterized by X-ray absorption near-edge structure (XANES) and X-ray photoelectron spectroscopy (XPS). Combined XANES Mo *L*-edge and XPS results revealed that the Mo 4*d* electronic level is not strongly influenced by the preparation procedures but that it is clearly modified by the presence of Pd. The splitting of 2.4−2.6 eV obtained in the white line at both Mo $L_{II,III}$-edges clearly indicated that Mo was tetrahedrally coordinated in all dehydrated catalysts. The Mo oxidation state, evaluated by the energy shift in the absorption edge, was also independent of the synthesis process. The Mo $L_{II}$-edge is discussed for the first time as a very sensitive probe to determine the nature of Mo species. Even the XANES $L_{III}$-edge relative intensity of the maximum at the split white line depends on the Mo coordination; at the $L_{II}$-edge, intensities do not depend on Mo coordination alone. This aspect should be associated, consistent with the binding energy (BE) of 3*d* levels observed by XPS, with the presence of Al atoms at the second Mo-surrounding in Mo-exchanged sites in zeolites.

## Introduction

Molybdenum-containing zeolites (Mo/HY, MoNaY, and Mo/USY) belong to one of the categories of catalysts widely used for hydrotreatment and hydrogenation reactions of oil fractions[1−7] and for the direct partial oxidation of $CH_4$ into $C_1$-oxygenates.[8,9] More recently, it has been reported that molybdenum oxides deposited on ZSM-5 zeolites in high dispersion produce catalysts that are active and selective in the dehydrogenation−aromatization of methane.[10−13] For all these systems, a high thermal and chemical stability of the zeolite is required because in such reactions molybdena catalysts operate at rather high temperatures: usually above 750 K. This requirement is fulfilled with zeolites Y (HY) and ZSM-5, which are sufficiently stable to withstand such conditions.[8] However, the micropore structure and low ion-exchange capacity of HY zeolite hinder the application of conventional methods to incorporate molybdenum precursors to the zeolite substrate.[4] Accordingly, other less common preparation methods have been developed. These include solid-state ion exchange using $MoCl_5$,[1,4,14] adsorption−decomposition of neutral $Mo(CO)_6$[15,16] complex, and impregnation with aqueous solutions of ammonium heptamolybdate followed by decomposition under reduced pressure.[1] Since these methodologies may vary the chemical environment, symmetry, and location of the molybdenum in the zeolite, and because these factors exert a strong effect on reactivity, precise knowledge of the chemical structures and electronic characteristics of Mo ions generated by the preparation method and pretreatment appears to be crucial.

Within this framework, X-ray absorption near-edge structure (XANES) and photoelectron spectroscopy (XPS) are extremely useful complementary characterization techniques. The former technique allows investigations of the local symmetry and electronic properties of absorbing atoms even when the species formed are present as amorphous and/or highly dispersed phases. The restricted escape depth of Mo photoelectrons in XANES at total electron yield (TEY) mode and in XPS experiments is responsible for the counting of Mo atoms at depths no greater than 5−7 nm.

XANES is associated with the excitation process of a core electron to unoccupied bounded states (below the ionization threshold) and to quasi-bound states interacting with the continuum (above or near the threshold). XANES contains information on the electronic state of the X-ray absorbing atom and on its surrounding local structure. There are many studies in the literature that report the successful accomplishment of XANES measurements at the Mo K-edges.[17−20] For that absorption energy (20000 eV), the $1s \rightarrow 4d$ preedge transitions are determined and used to reveal the symmetry around the Mo atom. In this case, if the symmetry group loses an inversion center (for example, on passing from the octahedral to the tetrahedral coordination or only distorting the octahedron), the 4*d* states can be hybridized with *np* oxygen states: the octahedral symmetry selection rule breaks down as soon as there is no longer a center of inversion symmetry in the Mo site. This will increase the probability intensity of the transition from the 1*s* to the 4*d* state because of the contribution of the *np* final state. Despite these helpful characteristics as tools for characterization, at the *K*-edge the XANES spectrum has an intrinsic resolution of approximately 5 eV. This is a disadvantage for good structural characterization when energy splitting smaller than 5 eV is to be observed, as in Mo splitting due to changes in Mo coordination.

An improved resolution of about 0.5 eV can be reached at the $L_{III,II}$ Mo-edges (around 2500 eV), which greatly enhances the structural characterization. Moreover, at this edge the *d*-orbital is directly involved with electronic bonding related to

* Corresponding author. E-mail: requejo@stm.lbl.gov.
[†] Departamento de Física, Facultad de Ciencias Exactas, UNLP, CC/67 1900 La Plata and IFLP(CONICET).
[‡] Instituto de Catálisis y Petroleoquímica, CSIC.
[§] Present address. Materials Science Division, LBNL, Mailstop 66-200, Berkeley, CA 94720.
[||] Fellow of UNLP.

10.1021/jp014648p CCC: $22.00 
Published on Web 07/19/2002

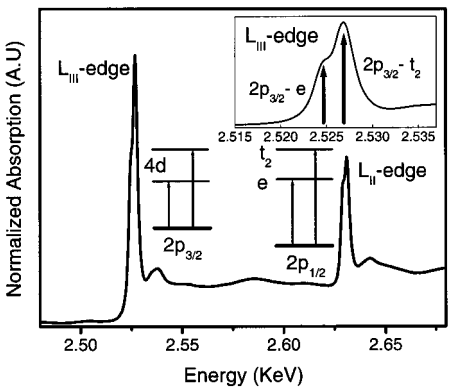


**Figure 1.** Mo XANES spectra of $Na_2MoO_4$ at $L_{III,II}$-edges. Insets show schematically the involved electronic levels.

catalytic processes (the *K*-edge is dominated by a final state *p*-character, which is not directly concerned with chemical bonds). Both the $L_{III}$- and $L_{II}$-edges describe the transitions from the 2*p* core state to the empty states of the *d*-band. In the case of 4*d* systems, the difference between the energy at $L_{III}$- and $L_{II}$-edges is of the order of 100 eV. The $L_{III}$ white line is originated when the transition proceeds from the $p_{3/2}$ core-level to a vacant *d* final state, while the electronic transition from $p_{1/2}$ level to the same *d*-band produces the $L_{II}$ white line.

In recent years, study of *L* absorption edge shapes has been employed in several works to establish the coordination and the *d*-band vacancies of the central atom. Lytle et al.[21,22] determined the relationships between the white line area at the Mo $L_{III}$-edge and the *d*-character in pure metals and in some third-row transition-metal complexes. George et al.[23] recorded the $L_{III}$-edges of molybdenum to analyze the unfilled *d*-level splitting in Mo compounds and enzymes. Evans and Mosselmans[24] studied the $L_{II-}$ and $L_{III}$-edge features in molybdenum complexes. After this, the local site symmetry of molybdenum oxides phases on MgO was determined by Bare et al.,[25] and more recently these studies have been extended by the same authors to Mo in oxide supports such as $Al_2O_3$ and $TiO_2$ measured under different in situ conditions.[26,27] Oyama et al. performed a very detailed study about supported Mo species on oxides at very low contents of Mo.[28] Only a few studies have been devoted to clarifying the origin of the different shapes of *L*-edges in Mo. The first spectra were published by Hedman et al.[29] Teo and Lee[30] showed that the contribution at $L_{II,III}$-edges has a predominantly *d*-character (50 times more than the $p-s$ transitions) and, more recently, de Groot[31,32] has offered an excellent analysis of the differences between the $L_{III}$ and $L_{II}$ absorption spectra in both 3- and 4*d* systems with octahedral symmetry. For $Mo^{6+}$ compounds, the variable splitting in the Mo $L_{II,III}$-edges reflects the ligand field splitting of the *d*-orbitals: in a tetrahedral field, the splitting between the *d*-levels ($t_2$ and *e*) is smaller than the splitting in an octahedral field ($t_{2g}$ and $e_g$). These transitions are illustrated schematically in Figure 1 for the $Na_2MoO_4$ system, where the only crystallographic site of Mo is tetrahedrally coordinated with oxygen atoms.

Despite the difficulties in experimentally calculating the white line areas at *L*-edges (the proximity of the $L_{III}$ extended X-ray absorption fine structure—EXAFS—region to the $L_{II}$ spectra complicate the edge-step and the preedge background subtraction), *L*-XANES spectroscopy is clearly a useful probe for characterizing electronic features in metal centers. In fact, as mentioned above XANES at the $L_{II,III}$ levels probes orbitals of *d*-character, which are the primary orbitals involved in bonding, and the fact that the number of the available orbitals at the unfilled Mo *d*-level is proportional to the white line area-intensity[18,31,32] affords an empirical method to analyze the unoccupied density of states of Mo. In sum, both the shapes and area of the white lines at *L*-edges in molybdenum systems allow one to analyze the Mo local symmetry and the degree of occupancy of the 4*d* electronic level.

In keeping with the above, incorporation of a second metal to the Mo-zeolite substrate should result in a change in the molybdenum symmetry and occupancy of the 4*d* level. Because palladium displays a high hydrogenation capacity in hydrogenation and hydrotreating reactions, here a set of binary palladium−molybdenum-containing zeolites was also prepared. For all the samples, XANES and photoelectron spectra were recorded with the aim of determining the effect of the preparation procedures on the chemical environment, symmetry, and electronic properties of Mo(VI) surrounded by oxide ions and whether these interactions are influenced by the incorporation of palladium.

## Experimental Section

**Catalyst Preparation.** *Mo/HY Series.* All catalysts were prepared from the original ultrastable HY zeolite (Conteka). The characteristics of the bare HY zeolite are as follows: $SiO_2/Al_2O_3$ molar ratio 5.6, $Na_2O$ content 0.14 wt %, and unit cell 2.454 nm. Three different methods: (i) impregnation with $Mo(CO)_6$ complex, (ii) solid−solid ion exchanges, and (iii) impregnation of HY zeolite with ammonium heptamolybdate were employed.

In method (i) HY zeolite was impregnated with the neutral $Mo(CO)_6$ (Merck, reagent grade) complex solubilized in benzene (Merck, HPLC grade). The thermal decomposition of $Mo(CO)_6$ is a complex process that occurs through attack of the carbonyl groups by surface OH groups bound to $Al^{3+}$ sites of the zeolite lattice according to eq 1:

$$Mo(CO)_6 + n\text{Al}-\text{OH} \rightarrow n\text{AlO}-\text{Mo}(CO)_{6-n} + {}^{n}/_{2}H_2 + n\text{CO} \quad (1)$$

This process is activated and courses at a high rate at temperatures above 573 K.[15] The adsorbed complex was decomposed under vacuum at 333 K and then dried in air at 383 K for 1 h. Finally, calcination was conducted at 723 K for 1 h in a glass tube. This sample will henceforth be referred to as Mo(CO).

In method (ii), the starting HY zeolite was grafted with $MoCl_5$ (Aldrich) precursor.[33] Before grafting, the HY zeolite was dehydrated in flowing He at 493 K for 2 h to minimize hydrolysis of $MoCl_5$ by the molecular water held by the zeolite, and then immediately mixed with anhydrous $MoCl_5$ and ground in a mortar and pestle. The resulting mixture was subsequently introduced into a flow reactor and heated in flowing He at 673 K for 6 h. In an oxygen-free environment, $MoCl_5$ becomes hydrolyzed on the zeolite hydroxyl groups according to eq 2:

$$MoCl_5 + n\text{Al}-\text{OH} \rightarrow \text{AlO}-MoO_x + \text{HCl} \quad (2)$$

After this pretreatment, the catalyst was dried at 383 K for 2 h and calcined at 723 K in air for 2 h. The resulting catalyst will be referred to as Mo(Cl).

The type (iii) procedure consisted of the incorporation of Mo to the HY zeolite by aqueous impregnation with $(NH_4)_6Mo_7O_{24}$ (Merck, reagent grade) in the excess of solution, followed by removal of excess water in a rotary evaporator. The impregnate was dried at ambient temperature in a vacuum for 8 h, then at 383 K for 16 h, and finally calcined at 773 K at a low and constant pressure ($4 \times 10^{-2}$ mbar) and an extended period of

**TABLE 1: Characterization Data of Mo/HY and Pd−Mo/HY Catalysts**

| catalyst | PdO [wt] | $MoO_3$ [wt] | BET [$m^2/g$] | PdO size [nm] | zeolite crystallinity [%] |
|---|---|---|---|---|---|
| HY | | | 662 | | 100 |
| Mo(CO) | | 3.7 | 426 | | 82.1 |
| Mo(Cl) | | 6.8 | 495 | | 64.8 |
| Mo(A) | | 8.5 | 382 | | 37.1 |
| Pd−Mo(CO) | 1.27 | 3.2 | 614 | 15.0 | 47.5 |
| Pd−Mo(Cl) | 1.09 | 6.7 | 451 | 12.4 | 35.1 |
| Pd−Mo(A) | 1.12 | 7.8 | 308 | 5.4 | 15.5 |

time of 800 h in a special reactor. This catalyst will be referred to as Mo(A). Further thermal treatment of the impregnates, according to the constant rate decomposition procedure,[1,34] allowed the redistribution of Mo within the lattice. This redistribution process has been explained assuming vaporization of $MoO_3$ by the reaction with water vapor according to eq 3:

$$MoO_{3(s)} + H_2O_{(v)} \leftrightarrow MoO_2(OH)_{2(v)} \quad (3)$$

Although the vapor pressure of $MoO_2(OH)_2$ is relatively low ($1.2 \times 10^{-7}$ bar at 793 K),[35] the fact that the Mo(A) sample was exposed to water vapor for a long period of time and the short distances at which diffusion became operative enable the establishment of an equilibrium and of a molybdenum distribution based on a vaporization−readsorption mechanism.[36] This mechanism is based on the assumption that at high temperatures—e.g., above 700 K— the $MoO_3$ mainly deposited on the external surface redisperses throughout the zeolite surface, except perhaps inside cavities in which steric hindrance may be important. Assuming a molecular size for $MoO_2(OH)_2$ similar to that of $MoO_3$ (0.51 nm), its entrance in the small cavities (sodalite and hexagonal prisms) could be controlled by diffusion at high temperatures, where the Mo species would be distributed in more heterogeneous sites.

*Pd−Mo/HY Series.* Aliquots of the three Mo/HY samples, prepared following procedures (i)−(iii), were then used to incorporate palladium (Pd−Mo/HY series). The Pd−Mo(A), Pd−Mo(CO) and Pd−Mo(Cl) samples were prepared by a two-step impregnation procedure described previously,[37] using $Pd(NO_3)\cdot 2H_2O$ solution (Fluka, reagent grade) of appropriate concentration to yield approximately 1 wt % Pd. The volume of solution-to-zeolite was 20. The suspension was maintained at 343 K for 4 h under vigorous stirring, after which the excess water was evaporated in a rotary evaporator at the same temperature. Subsequently, the impregnate was dried at 383 K for 4 h, and finally calcined in air at 573 K for 4 h.

**Catalyst Characterization.** *Chemical Analysis.* Palladium and molybdenum contents were determined by atomic absorption spectrometry using a Perkin-Elmer 3030 absorption instrument. The samples were solubilized in a mixture of HF, HCl, and $HNO_3$ and homogenized in a microwave oven at a maximum power of 650 W. The final metal loading in the monometallic and binary catalysts, expressed on a water-free basis, are given in Table 1.

X-ray powder diffraction. XRD patterns of the samples were recorded on a Seifert 3000P diffractometer with nickel-filtered Cu K$\alpha$ ($\lambda = 0.15418$ nm) radiation by scanning $2\theta$ angles ranging from 5 to 80°. Nitrogen adsorption isotherms were measured at 77 K using a Micromeritics Digisorb 2600 automatic apparatus on samples previously outgassed at 523 K. For comparative purposes, the isotherm of the plain HY zeolite was also obtained. The textural properties of Mo/HY and Pd−Mo/HY samples are also shown in Table 1.

*XANES Characterization.* Mo $L_{II}$- and $L_{III}$-edge XANES data were collected at the SXS beam line at the Laboratorio Nacional do Luz Sincrotron (LNLS), Campinas (Brazil). A Si (111) double-crystal monochromator with a slit aperture of 2.5 mm to obtain the desired high resolution of about 0.5 eV was used. Details of the experimental setup of the beam line have been published elsewhere.[38] The X-ray absorption spectra were recorded in total electron yield mode, collecting the emitted current, for each photon-energy, with an electrometer connected to the sample. Experiments were performed in a vacuum of $10^{-7}$ mbar at room temperature. The energy scale was calibrated setting the Mo $L_{III}$-edge, defined by the first inflection point, of the X-ray absorption spectrum of the Mo metallic foil sample to 2520 eV. The final TEY XANES spectra were obtained after background subtraction and normalization to the postedge intensity.

*XPS Analysis.* Photoelectron spectra were recorded on a VG Escalab 200R electron spectrometer equipped with a hemispherical electron analyzer and a Mg K$\alpha$ ($h\nu = 1253.6$ eV, 1 eV $= 1.603 \times 10^{-19}$ J) X-ray source. A PDP 11/04 computer (Digital Equipment Co.) was used to record and analyze the spectra. All samples were mounted on a manipulator, which allowed transfer from the preparation chamber to the analysis chamber. All samples were then outgassed at 623 K for 1 h prior to being moved to the analysis chamber. During data acquisition, residual pressure was kept below $3 \times 10^{-9}$ mbar. Each spectral region of the photoelectrons of interest was scanned a number of times to obtain a good signal-to-noise ratio. Peak intensities were estimated by calculating the integral of each peak and its fitting to a combination of Lorentzian/Gaussian lines of varying proportions. Although surface charging was observed on all the samples, accurate binding energies ($\pm 0.1$ eV) could be determined by charge referencing with the Si 2*p* peak of the aluminosilicate substrate at 102.7 eV. For each catalyst sample, Si 2*p*, Al 2*p*, Pd 3*d*, and Mo 3*d* peaks were recorded.

## Results and Discussion

**$N_2$ Adsorption−Desorption and XRD Data.** The different methods and precursors used in preparation of Mo/HY catalysts did not substantially alter the pore structure of HY zeolite. The shape of the $N_2$ isotherms (not shown here) for the all catalysts and the plain HY were quite similar and the form of their hysteresis loops indicates the presence of micropores. As expected, as compared with bare HY, the BET (Brunauer-Emmett-Teller) area decreased in the Mo/HY catalyst and this decrease was more pronounced for Pd−Mo(A) and Pd−Mo(Cl) zeolites.

Substantial changes in the crystallinity of the starting HY zeolite were also observed. It was found that crystallinity decayed by approximately 7% for the parent Pd/HY sample, but the decrease was much more important for the other binary catalysts (52.5, 64.9, and 84.5% for Pd−Mo(CO), Pd−Mo(Cl), and Pd−Mo(A), respectively) (Table 1). A less marked decrease in crystallinity was observed for Mo catalysts. The larger decrease in zeolite crystallinity in the binary PdMo/HY samples can thus be associated with the incorporation of Pd to the Mo/HY samples in the second impregnation step. The X-ray diffraction lines for the tetragonal phase of PdO, occurring at a *d* spacing of 0.2647, 0.5228, and 0.1335 nm (ASTM 41-1107), were observed in all samples (Table 1). From the corrected full width at half-maximum of these diffractions, the Debye−Scherrer equation revealed the smallest particle sizes of PdO for Mo(A) (5.4 nm) and the largest for Mo(CO) (14.5 nm)

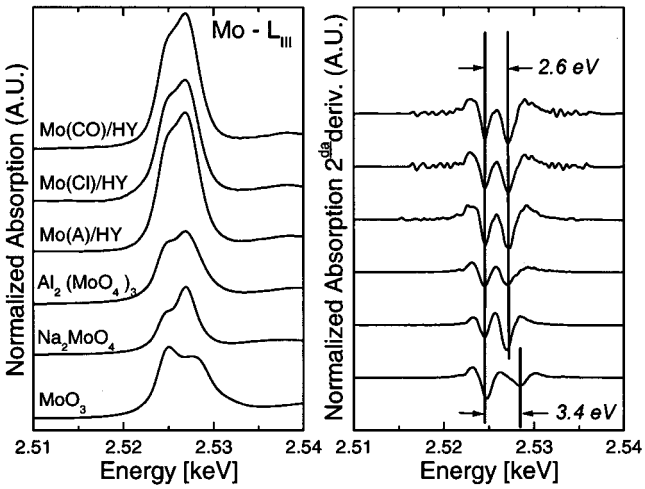


**Figure 2.** Mo $L_{III}$-edge XANES spectra (left) and second-derivative curves (right) for Mo/HY catalysts and reference compounds.

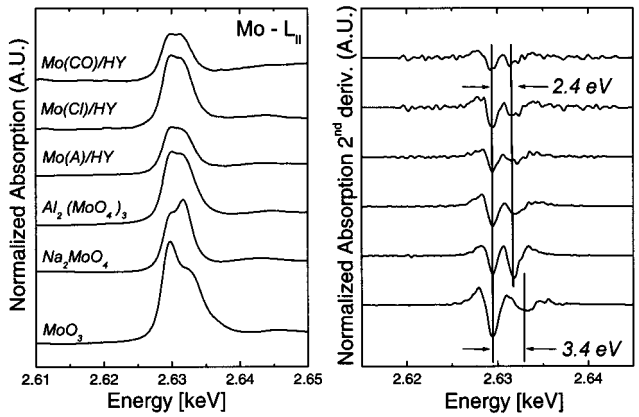


**Figure 3.** Mo $L_{II}$-edge XANES spectra (left) and second-derivative curves (right) for Mo/HY catalysts and reference compounds.

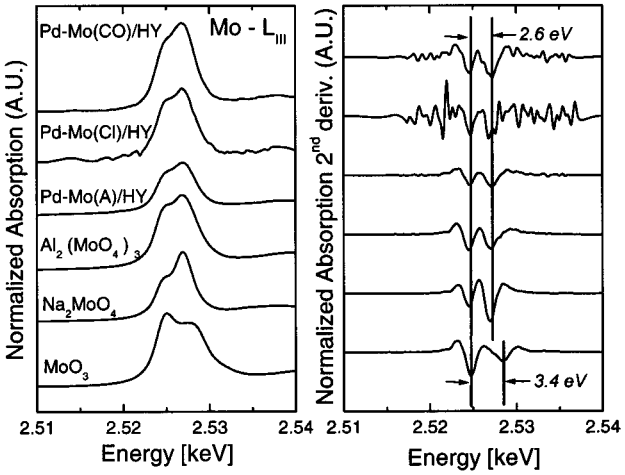


**Figure 4.** Mo $L_{III}$-edge XANES spectra (left) and second-derivative curves (right) for Pd−Mo/HY catalysts and reference compounds.

sample. The diffraction lines of the $MoO_3$ phase (ASTM 21-569) were absent in both Mo/HY and PdMo/HY samples.

**XANES Characterization.** The XANES TEY-mode spectra of Mo $L_{III}$ and $L_{II}$ X-ray absorption edges are shown in Figures 2 to 5, and the calculated splitting and white line intensity area values are offered in Table 2 and Figure 6. The first evident consequence derived from the spectra is the fact that there is no edge shifting of the Mo-edge in any of the catalysts, i.e., the oxidation state of Mo is the same.

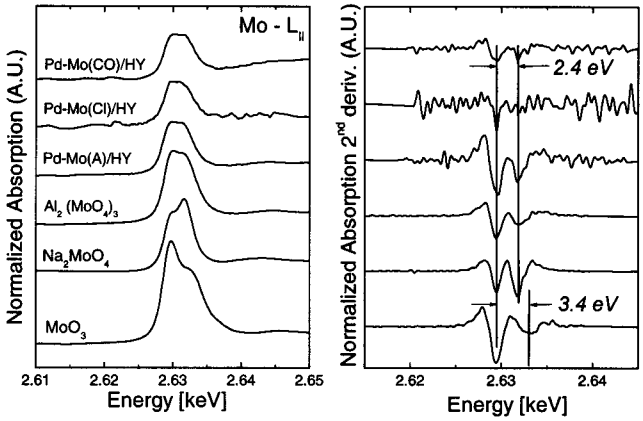


**Figure 5.** Mo $L_{II}$-edge XANES spectra (left) and second-derivative curves (right) for Pd−Mo/HY catalysts and reference compounds.

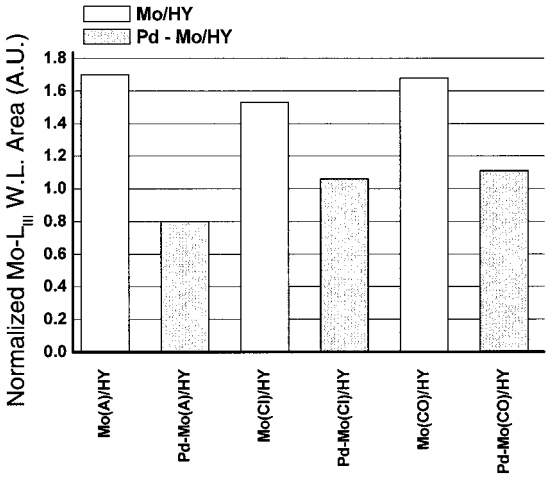


**Figure 6.** Normalized Mo $L_{III}$ white line intensity area in Mo/HY (white bars) and Pd−Mo/HY catalysts (shadow bars). The Mo $L_{III}$ white line area was normalized with respect to the Mo $L_{III}$ white line measured in $Al_2(MoO_4)_2$ reference compound.

**TABLE 2: Normalized White Line Area and Energy Splitting at the Mo $L_{III}$-Edge in Mo/HY and Pd−Mo/HY Catalysts and Reference Compounds**

| sample | normalized area[a] | splitting [eV][b] |
|---|---|---|
| $MoO_3$ | 1.14 | 3.6 |
| $Na_2MoO_4$ | 0.78 | 2.4 |
| $Al_2(MoO_4)_3$ | 1.00 | 2.4 |
| Mo(A) | 1.70 | 2.4 |
| Mo(Cl) | 1.53 | 2.6 |
| Mo(CO) | 1.68 | 2.4 |
| Pd−Mo(A) | 0.80 | 2.6 |
| Pd−Mo(Cl) | 1.06 | ∼2.4 |
| Pd−Mo(CO) | 1.11 | ∼2.6 |

[a] Normalized with respect to $L_{III}$ white line area of $Al_2(MoO_4)_3$. [b] Measured at the second derivate spectra

The atomic-like electric dipole transitions from the $2p_{3/2}$ and $2p_{1/2}$ initial states to the $4d$ final state produce, at the $L_{III-}$ and $L_{II}$-edges, respectively, the large white lines observed. In all cases, the white line at the Mo $L_{III,II}$-edges are split into a doublet. This can be interpreted as being due to a ligand field splitting of the final state *d*-orbitals.[23,25,27,31] For tetrahedral symmetry, the magnitude of the splitting is less that in the octahedral field ($e$,$t_2$ split versus $t_{2g}$,$e_g$ split). In particular, the range of values for the splitting at the Mo $L_{III}$-edge is 1.8−2.6 eV for tetrahedrally coordinated Mo, and 3.1−4.5 eV for Mo octahedrally coordinated to oxide anions ($O^{2-}$). A similar

splitting can be observed at the Mo $L_{II}$-edge.[25] Figures 2 and 3 summarize the $L_{III}$- and $L_{II}$-edge data and the respective second derivative spectra on Mo reference compounds and the different Mo/HY catalysts, while Figures 4 and 5 show the same for Mo/HY catalysts containing Pd (Pd−Mo/HY). The splitting values are reported in Table 2. In all cases, according to the splitting the Mo symmetries (Figures 2−6) clearly correspond to molybdenum atoms in a tetrahedral environment (*e* and $t_2$ transitions).

The number of available orbitals is reflected in the relative intensity of the two $L_{II}$- and $L_{III}$-edge adsorption features. The relative intensity ratios of the white lines at the $L_{III,II}$-edges can be predicted through simple ligand field theory. It has been also reported that for Mo atoms with octahedral symmetries, the main reason for the difference between the $L_{III}$- and $L_{II}$-edges is in fact the multiplet effects coupling the 2*p* core-level wave function to the valence state of 4*d* character.[31] To our knowledge, no similar analysis has been performed for tetrahedral Mo symmetries. At the Mo $L_{III}$-edge in compounds with octahedrally coordinated Mo, the first maximum is higher than the second, and *vice versa* for tetrahedrally coordinated Mo. In other words, at the Mo $L_{III}$-edge, $e > t^2$ and $t_{2g} > e_g$. This can be observed in different previous works [25,26,28,39,40] and also in our Mo $L_{III}$-edge data (Figures 2 and 4).

With respect to the WL intensity differences between Mo−HY samples and reference compounds, the fact that the WL intensity in catalysts without Pd is higher than in the standard compounds could be connected with the stabilization of small Mo oxide species interacting with exchange sites in the HY zeolite cages. The same result was already reported for Mo-ZSM5 zeolites[39] and we also experimentally observed the same trend (i.e., the higher WL intensity) for MoOx species in zeolites for Mo-H-ZSM11 and Mo-H-BEA catalysts (results not reported yet).

Fortunately, in this work it can also be seen that the intensity feature at the Mo $L_{II}$-edge not only depends on the Mo-coordination as occurs in the $L_{III}$ case. In fact, Figures 4 and 6 show that different features can be observed at the Mo $L_{II}$-edges between the references $Al_2(MoO_4)_2$ and $Na_2MoO_4$, both having the same coordination (tetrahedral) of Mo atoms to $O^{2-}$ anions. For clarity, Figure 7b shows the Mo $L_{II}$-edge experimental XANES spectra for $Al_2(MoO_4)_2$ and $Na_2MoO_4$ separately, indicating the corresponding *e* and $t_2$ transitions. In all catalysts measured, the same features as those observed in the $Al_2(MoO_4)_3$ case at the $L_{II}$-edge can be distinguished, i.e., the first maximum (*e* transition) is more intense than the second one ($t_2$ transition), even in Mo with a tetrahedral environment. Although we do not have a model to describe the shape at the Mo $L_{II}$-edge in these cases, a simple interpretation can be attempted. Thus, if Mo atoms are located at exchange zeolite sites, aluminum atoms should modify the electronic charge density and/or the Mo-surrounding geometric characteristics via Al−O−Mo bonding (as in the $Al_2(MoO_4)_3$ reference compound). In view of that, Mo atoms highly dispersed in samples should be bonded with oxygen, with Al as a close neighbor, which probably means that Mo is at exchange sites in the zeolites. According to this interpretation, some predictions from calculations based on FEFF8[41] can be made in good agreement with the experimental results. This version of the code includes self-consistent potentials, a better treatment of relativistic effects, and a more accurate calculation of the edge position and shape than other codes or previous versions of the same code. This code is being applied successfully to studies of *L*-edge XANES spectra in Pt-based systems,[42,43] affording a good tool for approaching with a model of a cluster with Mo as the central absorbing atom. Figure 7 shows our simulations at the Mo $L_{II,III}$-edge for $Al_2(MoO_4)_3$ (for Mo site with four oxygen nearest neighbors) and $Na_2MoO_4$ reference compounds. The experimental tendency observed between the intensities at the *e* and $t_2$ transitions at $L_{III}$ (Figure 7a,b) and $L_{II}$ (Figure 7c,d) edges can be qualitatively reproduced by simulation with FEFF8 code. In effect, clusters of about 5 Å radius diameter (including around 30 atoms, up to the 4 nearest atomic shells from the Mo, considered as central atom) can be proposed to simulate the XANES spectra with full multiple scattering calculations using FEFF8 code. It is significant to note that the identical set of parameters for the simulation can reproduce both experimental XANES Mo $L_{II}$ and $L_{III}$ absorption spectra tendencies. Even a detailed study should be performed for a better agreement between experiment and simulation; this is the first result that shows the same qualitative trend between experiment and theory. Despite these considerations, the origin of this singular high of the maxima at the $L_{II}$-edge splitting is not completely understood and remains as an open question in the present contribution and will be revisited in a future work.

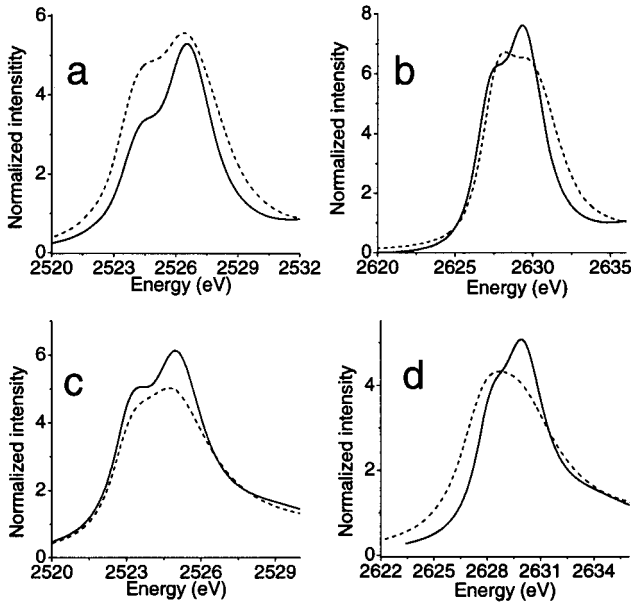


**Figure 7.** Experimental (*a* and *b*) and simulated (*c* and *d*), using FEFF8 code,[41] XANES spectra at Mo $L_{III}$-(*a* and *c*) and $L_{II}$- (*b* and *d*) edges. Solid line corresponds to $Na_2MoO_4$ and dotted line corresponds to $Al_2(MoO_4)_3$. First peak corresponds to $2p \rightarrow e$ electronic transition while the second peak corresponds to $2p \rightarrow t_2$ (see Figure 1).

The normalized $L_{III}$ intensity area allows analysis of the electronic occupancy at the Mo 4*d*-level. The $L_{II}$-edge jump is one-half of the $L_{III}$-edge jump and is overlapped on the $L_{II}$ region. At $L_{II}$-edge the removal of the background contribution and the normalization of the spectrum is more difficult than in the $L_{III}$ case. For these reasons, analysis of the white line intensity area is performed in the white line at the $L_{III}$-edge. All spectra with the prominent feature at the white lines in both $L_{III,II}$-edges are shown in Figures 2 to 6. Table 2 shows the normalized white line areas at the $L_{III}$-edge. The $L_{III}$ white line intensity in $Al_2(MoO_4)_3$ was considered a reference (unit area). The main feature of the intensity areas in the samples can be detected readily by comparing the Mo/HY samples (Figure 2) and Pd−Mo/HY samples (Figure 4). In fact, this feature—shown in Figure 6—allows us to determine a systematic effect of Pd on the samples. In all cases, the presence of Pd diminishes the white line intensity in the corresponding increases when Pd is

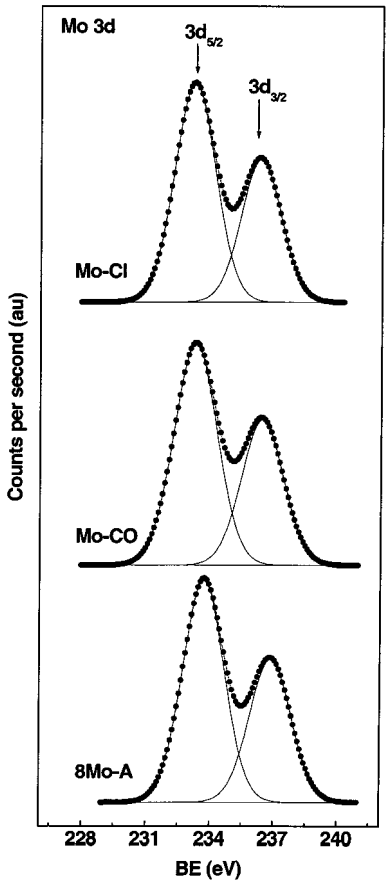


**Figure 8.** Mo 3*d* core-level spectra of Mo-loaded HY zeolite samples outgassed at 623 K.

present in the sample. In other words, the density of unoccupied states in Mo atoms decreases with the incorporation of Pd.

This variation in the white line intensity due to the incorporation of Pd does not necessarily imply that Pd and Mo are bonded directly. The electronic configuration at Mo nearest neighborhood could change simply by variations in the charge of oxygen atoms, as in Mo−O−Pd bonds. Moreover, no evidence of Mo−Pd bonds is present from any of the characterizations performed. The present modification of the white line reported here is the only effect we were able to detect in the Pd−Mo/HY samples. Another undesirable effect that affects the experimental XANES spectra owing to the incorporation of Pd, such as the increase in the conductivity of the samples, must be discarded since all the data treated were normalized and the background signal was subtracted in order to eliminate any alteration in the analysis of the data. An understanding of the relationship between Mo and Pd must be further elucidated using, for instance, EXAFS spectroscopy, but the evidence above indicates, at least, that some effect from Pd on Mo 4*d* level exist.

**XPS Characterization.** Photoelectron spectroscopy was used to elucidate the chemical nature and surface exposure of the Pd and Mo species in the calcined samples. Figures 8 and 9 show the Mo 3*d* core-level spectra of the in situ dehydrated Mo/HY and Pd−Mo/HY samples, respectively. The binding energies of the Mo $3d_{5/2}$ and Pd $3d_{5/2}$ peaks together with the Pd/Si and Mo/Si atomic ratios of dehydrated Mo/HY and Pd−Mo/HY samples are summarized in Table 3. All spectra of the $Mo^{6+}$ ions display the spin−orbit splitting of Mo 3*d* core-levels (ca. 3.1 eV) like that observed in $MoO_3$ and $Al_2(MoO_4)_3$ compounds.[44] As can be seen in Figures 8 and 9, the resolution of the Mo 3*d* core-levels is quite good, and their full width at half-maximum (fwhm) is ca. 2.3 eV. No significant changes in the Mo 3*d* line shape or in fwhm were observed in the binary PdMo systems. The broadening of Mo 3*d* peaks has been attributed to several factors including: (i) electron-transfer between molybdenum and the support; (ii) the presence of more than one type of $Mo^{6+}$ species with different chemical characteristics which cannot be disclosed by XPS; and (iii) differential charge, stemming from poorly conductive samples.[45] In this work, however, the contribution of factor (iii) can, in principle, be ruled out because no similar broadening was observed in the Al 2p peak. Thus, peak broadening would be considered to be due to factors (i) and (ii). It is well established that at low loading the dominant Mo oxide species that remain in a highly dispersed state have tetrahedral coordination.[44,46] However, as loading increases, other species with octahedral coordination form as a function of the Mo loading and eventually a bulk $MoO_3$ phase is formed at a sufficiently high loading. This is not the case of Mo/HY (and also Pd−Mo/HY) catalysts because the energy splitting of ca. 2.4 eV at the XANES Mo $L_{III}$-edge spectra in Mo/HY catalysts (Table 2) precludes the formation of octahedrally coordinated Mo structures. We therefore believe than that molybdenum oxides may adopt different environments depending on the location of the anchoring site while in all of them the tetrahedral structure, more or less distorted, is preserved. Additional spectra of the Mo/HY zeolites outgassed at ambient temperature showed the BE of the Mo $3d_{5/2}$ peak at

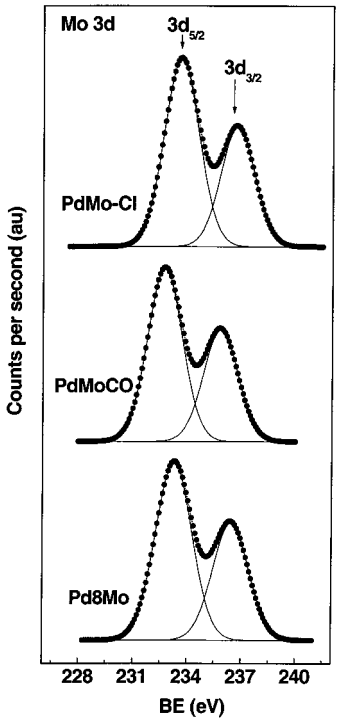


**Figure 9.** Mo 3*d* core-level spectra of PdMo-loaded HY zeolite samples outgassed at 623 K.

**TABLE 3: Binding Energy of Core Electrons (eV) and Surface Atomic Ratios of Dehydrated Mo/HY and Pd−Mo/HY Catalysts**

| catalyst | Pd $3d_{5/2}$ | Mo $3d_{5/2}$ | Pd/Mo | Mo/Si atom |
|---|---|---|---|---|
| Mo(CO) | | 233.4 | | 0.102 (0.047)[a] |
| Mo(Cl) | | 233.4 | | 0.129 (0.086)[a] |
| Mo(A) | | 233.2 | | 0.137 (0.107)[a] |
| Pd−Mo(CO) | 336.9 | 233.3 | 0.11 | 0.065 (0.040)[a] |
| Pd−Mo(Cl) | 337.0 | 233.2 | 0.23 | 0.109 (0.085)[a] |
| Pd−Mo(A) | 336.9 | 233.2 | 0.30 | 0.105 (0.098)[a] |

[a] Mo/Si ratios provided by chemical analysis are in parentheses

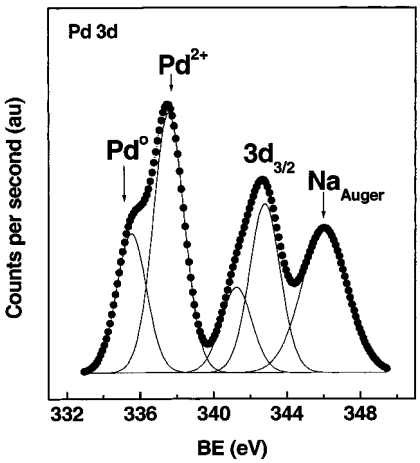


**Figure 10.** Pd 3*d* core-level spectrum of the representative Pd−Mo(Cl) zeolite sample outgassed at 623 K.

233.2 ± 0.1 eV, suggesting that molybdenum coordination is preserved upon outgassing, both at ambient temperature and at 623 K. The electron-transfer process might be also involved, at least to a certain extent. However, the almost constancy of the BE values within the composition range explored suggests minor electronic interactions, if any, in supported Mo/HY (and Pd−Mo/HY) zeolites.

The Pd 3*d* core-level spectrum of the representative Pd−Mo(Cl) sample is depicted in Figure 10. This spectrum was resolved in two doublets, corresponding to both $Pd^{2+}$ ions (BE Pd $3d_{5/2}$ = 336.9 eV) species in an environment of oxide anions[47] and $Pd^{o}$ (BE Pd $3d_{5/2}$ = 535.5 eV) in Pd clusters. A common feature of the Pd 3*d* line profile, shown in Figure 10, is that the binary PdMo samples show a broad component in the region of high BE energies overlapping with the Pd$3d_{3/2}$ peak at ca. 343.7 eV. This broad peak may be originated by the overlapping of the secondary $Na_{KLL}$ Auger line. As mentioned in the Experimental Section, the Na content of the original zeolite is 0.14 wt %, expressed as $Na_2O$. The binding energy of the most intense Mo $3d_{5/2}$ peak at 233.2−233.4 eV is essentially the same for all catalysts and is somewhat higher than the value expected for crystalline $MoO_3$ and closer to $Al_2(MoO_4)_3$.[44]

An examination of the Mo/Si ratios derived from XPS and their comparison with the Mo/Si ratios derived from chemical analyses indicates that molybdenum is quite well dispersed within the lattice. The decrease in Mo/Si ratios for the binary PdMo/HY systems, and particularly for Pd−Mo(CO), with respect to the Mo/HY counterparts indicates that the process of Pd incorporation alters the molybdenum distribution to a significant extent. The slight decrease in the Mo content in the binary systems suggests that some Mo incorporated in the preparation of Mo/HY systems became solubilized during the Pd impregnation step. It is presumed that this solubilization of the molybdenum species occurs preferentially in locations in which no high dispersion was reached during the incorporation of Mo in the monometallic Mo/HY systems.

As we have already shown, Mo XPS binding energies do not reflect the same behavior that XANES white line analysis. To understand this, one must bear in mind that the energies involved for each case are different. While the photoelectron Mo 3*d* is a core level, the perturbation detected by the XANES only affects the Mo orbitals close to the valence band (empty states). The energies involved in the two processes differ in more than 1 order of magnitude.

## Conclusions

The local site coordination of molybdenum incorporated in a set of Mo/HY and Pd−Mo/HY catalysts has been established using XANES spectroscopy at the Mo $L_{II,III}$-edges and XPS. No changes in the hexavalent Mo oxidation state were observed in the samples.

The obtained splitting of 2.4−2.6 eV at both Mo $L_{II,III}$-edges clearly indicates that Mo is tetrahedrally coordinated in all catalysts. Similarly, the BE of Mo $3d_{5/2}$ core-level spectra at ca. 233.2 eV revealed that Mo atoms are in tetrahedral coordination in a very high dispersion degree. While the Mo $L_{III}$-edge reflects the expected behavior, at the $L_{II}$-edge the intensity feature of the split peaks of the white line does not depend on the Mo coordination alone. The electronic *e* transition is more intense than $t_2$.

All these experimental observations and calculations performed via simulations of the Mo $L_{II}$-edge XANES spectra based on a FEFF8 code strongly suggest that Al atoms are present at the near Mo surrounding, which can modify the electronic charge density and/or the geometry at the Mo site. This inversion in intensity between the two peaks at the white line, with respect to the Mo reference compounds (excepting $Al_2(MoO_4)_2$), is not observed the at the $L_{III}$-edge, $L_{II}$ being the only edge clearly affected in this shape.

The normalized $L_{III}$ intensity area allows analysis of the electronic *4d*-level occupancy in Mo. Although the origin of the different white line intensities at the Mo *L*-edge in Mo/HY catalysts should be addressed in future work, our results show that the electronic characteristics at the Mo 4*d* level should be different even when the Mo coordination is the same for all Mo atoms in the HY zeolite. In addition, we report for first time the Mo $L_{II}$-edge as a very suitable probe for the study of highly dispersed Mo species.

**Acknowledgment.** This work was partially supported by LNLS, Campinas SP, Brazil (under Project SXS 585/99), Fundación Antorchas (Argentina) and PEI 0132/98 (CONICET, Argentina). The authors acknowledge Flavio Vicentin for his technical assistance at SXS beam line. B.P. is indebted to the CAM (Spain) and European Community for a fellowship.

## References and Notes

(1) Fierro, J. L. G.; Conesa, J. C.; Lopez Agudo, A. *J. Catal.* **1987**, *108*, 334.
(2) Cid, R.; Orellana, F.; Lopez Agudo, A. *Appl. Catal.* **1987**, *32*, 327.
(3) Leglise, J.; Janin, A.; Lavalley, J. C.; Cornet, D. *J. Catal.* **1988**, *114*, 388.
(4) Anderson, J. A.; Pawelec, B.; Fierro, J. L. G. *Appl. Catal.* **1993**, *99*, 37.
(5) Anderson, J. A.; Pawelec, B.; Fierro, J. L. G.; Arias, P. L.; Duque, F.; Cambra, J. F. *Appl. Catal.* **1993**, *99*, 55.
(6) Welters, W. J. J. Zeolite supported metal sulfides as catalysts for cracking. Ph.D. dissertation, Eindhoven institute of Technology, 1994.
(7) Vasudevan, P. T.; Fierro, J. L. G. *Catal. Rev.—Sci. Eng.* **1996**, *38* (2), 161 and references therein.
(8) Bañares, M. A.; Pawelec, B.; Fierro, J. L. G. *Zeolites* **1992**, *12*, 882.
(9) Antiñolo, A.; Cañizares, P.; Carrillo, F.; Fernandez-Baeza, J.; Funez, F. J.; de Lucas, A.; Otero, A.; Rodriguez, L.; Valverde, J. L. *Appl. Catal. A: General* **2000**, *193*, 139.
(10) Wang, D.; Lunsford, J. H.; Rosynek, M. P. *Topics Catal.* **1996**, *3*, 289.
(11) Solymosi, F.; Csrényi, J.; Szoke, A.; Bánsági, t.; Oszko, A. *J. Catal.* **1997**, *165*, 150.
(12) Liu, S.; Dong, Q.; Ohnishi, R.; Ichikawa, M. *J. Chem. Soc., Chem. Commun.* **1997**, 1445.
(13) Li, W.; Meitzner, G. D.; Borry, R. W., III; Iglesia, E. *J. Catal.* **2000**, *191*, 373.
(14) Cid, R.; Gil Llambias, F. J.; Fierro, J. L. G.; Lopez Agudo, A.; Villaseñor, J. *J. Catal.* **1984**, *89*, 478.

(15) Abdo, S.; Howe, R. F. *J. Phys. Chem*. **1984**, *87*, 1713.
(16) Ward, M. B.; Lunsford, J. H. In *Proceedings of the 6th International Conference on Zeolites;* Olson, D. A., Bisio, A., Eds.; Butterworths: Guildford, 1984; p 405.
(17) Cramer, S. P.; Hodgson, K. O.; Gillium, W. O.; Mortenson, L. E. *J. Am. Chem. Soc*. **1978**, *100*, 3398.
(18) Takenaka, S.; Tanaka, T.; Funabiki, T.; Yoshida, S. *J. Phys. Chem. B* **1998**, *102*, 2960.
(19) Imamura, S.; Saski, H.; Shono, M.; Kanai, H. *J. Catal*. **1998**, *177*, 72.
(20) Shido, T.; Asdakura, K.; Noguchi, Y.; Iwasawa, Y. *Appl. Catal. A: General* **2000**, *194*−*195*, 365.
(21) Lytle, F. W. *J. Catal*. **1976**, *43*, 376.
(22) Lytle, F. W.; Wei, P. S. P.; Gregor, R. B.; Via, G. H.; Sinfelt, J. H. *J. Chem. Phys*. **1979**, *70*, 4849.
(23) George, G. N.; Cleland, W. E., Jr.; Enemark, J. H.; Smith, B. E.; Kipke, C. A.; Roberts, S. A.; Cramer, S. P. *J. Am. Chem. Soc*. **1990**, *112*, 2541.
(24) Evans, J.; Mosselmans, F. W. *J. Phys. Chem*. **1991**, *95*, 9673.
(25) Bare, S. R.; Mitchell, G. E.; Maj, J. J.; Vrieland, G. E.; Gland, J. L. *J. Phys. Chem*. **1993**, *97*, 6048.
(26) Hu, H.; Wachs, I. E.; Bare, S. R. *J. Phys. Chem*. **1995**, *99*, 10897.
(27) Bare, S. R. *Langmuir* **1998**, *14*, 1500.
(28) Radhakrishnan R.; Reed, C.; Oyama, S. T.; Seman, M.; Kondo, J. N.; Domen, K.; Ohminami, Y.; Asakura, K. *J. Phys. Chem. B* **2001**, *105*, 8519.
(29) Hedman, B.; Penner Hahn, J. E.; Hodgson, K. O. *EXAFS and Near Edge Structure III*; Hedman, B., Penner Hahn, J. E., Hodgson, K. O., Eds; Springer-Verlag: New York, 1984.
(30) Teo, B. K.; Lee, P. A. *J. Am. Chem. Soc*. **1979**, *101*, 2815.
(31) De Groot, F. M. F.; Hu, Z. W.; López, M. F.; Kaindi, G.; Guillot, F.; Tronc, M. *J. Chem. Phys*. **1994**, *101* (8), 6570.
(32) De Groot, F. M. F. *Physica B* **1995**, *208*−*209*, 15.
(33) Johns, J. R.; Howe, R. F. *Zeolites* **1985**, *5*, 251.
(34) Fierro, J. L. G.; Rojo, J. M.; Sanz, J. *Colloids Surf*. **1985**, *15*, 75.
(35) Sonnemans, J.; Mars, P. *J. Catal*. **1973**, *31*, 209.
(36) Leyrer, J.; Zaki, M. I.; Knozinger, H. *J. Phys. Chem*. **1986**, *90*, 4775.
(37) Pawelec, B.; Navarro, R.; Fierro, J. L. G.; Cambra, J. F.; Zugazaga, F.; Güemez, M. B.; Arias, P. L. *Fuel* **1997**, *1*, 61.
(38) Abbate, M.; Vicentin, F. C.; Compagnon-Cailhol, V.; Rocha, M. C.; Tolentino, H. *J. Synchr. Rad*. **1999**, *6*, 964.
(39) Requejo, F. G.; Lede, E. J.; Pierella, L. B.; Anunziata, O. A. *Surf. Sci., Catal.* **2001**, Nro. 135.
(40) Aritani, H.; Fukuda, O.; Miyaji, A.; Hasegawa, S. *Appl. Surf. Sci*. **2001**, *180*, 261.
(41) Ankudinov, A. L.; Ravel, B.; Rehr, J. J.; Conradson, S. D. *Phys. Rev. B* **1998**, *58*, 7565.
(42) Ankudinov, A. L.; Rehr, J. J.; Low, J. J.; Bare, S. R. *J. Synch. Rad.* **2001**, *8*, 578.
(43) Ankudinov, A. L.; Rehr, J. J.; Low, J. J.; Bare, S. R. *Phys. Rev. Lett*. **2001**, *86* (8), 1642.
(44) Borry, R. W., III; Kim, Y. H.; Huffsmith, A.; Reimer, J. A.; Iglesia, E. *J. Phys. Chem. B* **1999**, *103*, 5787.
(45) Zingg, D. S.; Makovsky, L. E.; Tischer, R. E.; Brown, F. R.; Hercules, D. M. *J. Phys. Chem.* **1980**, *84*, 2898.
(46) Nag, N. K. *J. Catal*. **1986**, *92*, 432.
(47) Briggs, D.; Seah, M. P. *Practical Surface Analysis by Auger and X-ray Photoelectron Spectroscopy*; Wiley: Chichester, 1983.